JREE: Vol. 3, No. 1, (Winter 2016) 8-16

Journal of Renewable Energy and Environment

Research Article

Journal Homepage: www.jree.ir

Numerical Investigation on Contaminant Dispersion from a Source over the Blocks in Steady and Unsteady Flows

M. Ziaei-Rad[a]*, I. Samea[b]

[a]*Department of Mechanical Engineering, University of Isfahan, Isfahan, Iran*
[b]*Department of Mechanical Engineering, Shahrekord University, Shahrekord, Iran*

PAPER INFO

Paper history:
Received 25 January 2015
Accepted in revised form 03 November 2015

Keywords:
Contaminant dispersion
Blocks
Unsteady flow
Numerical study

ABSTRACT

This paper deals with numerical study of semi-finite incompressible flow of air over two blocks with different heights in the presence of a condensing-source, dispensing- contaminant in the flow, in both steady and unsteady states. The numerical solution of governing PDE equations are constructed by a finite-volume method applied on structured grid arrangement. The effects of air flow velocity, contaminant source length and position, and the blocks height ratio on the concentration distribution, the mass transfer level and the time of transportation are studied. The results indicate that by increasing the inflow Reynolds number, the amount of contamination reaching the blocks and also the amount remaining between them decrease, while the mass transfer rate increases. It is shown that the closer the contaminant source to the blocks, the higher the mean concentration accumulating between the two blocks. It is also found that increasing the blocks' height ratio makes an ascending trend to the time for the arrival of contaminant to the blocks' walls, though the slopes of time-lines are different for each case.

1. INTRODUCTION

Investigating the unsteady dispersion of the contamination in cases the time of dispersion is important is a widespread issue. In many urban environments, where the pollution or fires disperse from a source and the wind pervades them, it is vital to know the time the hazard reaches the surrounding buildings. Furthermore, some chemical interactions, in which the interacting fluid requires electrodes, visibly cause contaminant dispersion in the fluid, and this leads to the possibility of contamination accumulation on the electrode plate. The duration and the way of dispersing contamination have some effects on the interaction. As a result, studying such issues can be advantageous. In order to calculate the time parameter, it is necessary to solve the concentration equation in the unsteady state.

The mass transfer around a surface with mounted obstacles is usually investigated in two different situations. In the first one, the obstacles are assumed to be larger than the near wall viscous layer, thus the flow fluctuations caused by such large obstacles propagate outside the viscous layer. In this case, to engage the problem, an appropriate velocity profile should be specified at the upstream boundary. In the second case, the obstacles lay inside the flow viscous layer. The examples are a micro electrode mounted on a conducting wall, or small buildings against the air front. A linear velocity profile is employed as upstream boundary condition in this case, to study the hydrodynamic problems. This paper deals with cases in which, the near wall velocity fluctuations do not affect the mean velocity profile, while still have an effect on the mass transfer. Boum et al. [1] studied numerically the laminar mass transfer on a plane surface (electrode) deformed by a square micro-obstacle by simulating the flow and mass transfer at the solid-liquid interface. The obstacle has the same order of magnitude as the diffusion layer thickness, so a linear approximation for the velocity profile is used at the inlet flow section. It has been shown that the velocity profile in the normal direction is disturbed in no more than three times the obstacles height. Moreover, the recirculating vortex behind the obstacle has been formed to have a copious effect on the mass transfer. Hancu et al. [2] modeled the fluid and mass transport processes in a straight channel with flow control obstructions is embedded in the

*Corresponding Author's Email: m.ziaeirad@eng.ui.ac.ir (M. Ziaei-Rad)

channel. Salt solutions are used to investigate the contamination transport and the dispersion of the salt.
Hayashi *et al.* [3] performed CFD analysis to examine the characteristics of the contaminated indoor air ventilation in a simplified two-dimensional room model. They studied the contaminant profile at different velocities. In addition, they used IECI and other factors to examine the characteristics of the contamination inhalation by an occupant in the room in details for some common human postures. Gadgil et al. [4] performed CFD simulations to investigate the relationship between the pollutant mixing time and the source location. Seventeen source locations and five blower configurations have been investigated. Results demonstrate extent dependency of the mixing time on the room airflow, and some dependency on the source location. They also explored the dependency of the mixing time on the velocity and the intensity of turbulence at the source location. Kaya et al. [5] undertook an experimental and numerical study on the heat and mass transfer analysis during drying of kiwifruits. In the experimental part, the effects of various drying conditions in terms of air velocity, temperature and relative humidity on drying characteristics of kiwifruits have been investigated. In addition, the time-dependent temperature and moisture distributions for different cases are obtained using a code developed to investigate heat and mass transfer aspects inside the fruits. Qi-Hong Deng [6] investigated the characteristics of the airflow and heat/contaminant transport structures in the indoor air environment by means of a convection transport visualization technique. Laminar double diffusive mixed convection in a two-dimensional displacement ventilated enclosure with discrete heat and contaminant sources has been numerically studied. Clear et al. [7] certified the elaboration of current convective heat transfer coefficient correlations. A clear limitation of these in situ experiments is their demands for taking into account all of the parameters that can affect the evaluation of the studied coefficient. As stated by the last cited researcher, an important issue is the evaluation of the radiative exchange between the wall surfaces and the sky since no accurate correlation is available. By imposing the boundary conditions, computational fluid dynamics (CFD) simulation benefits to avoid this limitation and with the increment of the computational resources, it becomes a valuable alternative way of evaluating the airflows around the buildings and, as a consequence, the external convective heat transfer coefficients. Kaya et al. [8, 9] studied the forced-air drying of some rectangular and cylindrical moist products. In such studies, the commercial CFD code solutions for the external flow of drying air was added to the code solving transient temperature and moisture distributions inside the moist products. J. Xamán *et al.* [10] analyzed the heat and mass transfer of an Air-Carbon Dioxide mixture (CO_2) inside a ventilated cavity in the laminar flow regime. In their study, the main purpose was to investigate how the concentration is distributed at different Reynolds numbers, with respect to the two obstacles considered existing against the fluid flow. Pal et al. [11] work was to investigate the characteristics of the airflow and heat/contaminant transport structures in the indoor air environment by means of a convection transport visualization technique. Their attentions were given to analyze the effects of the main factors, such as the strength of the heat source, the strength of the contaminant source, the strength of ventilation, and the ventilation mode.
Despite some experimental and numerical studies carried out on the contaminant dispersion in the steady state condition, specific studies have not been reported in the literature on the unsteady dispersion from a source of contamination.
In this study, the main purpose is to investigate how the concentration is distributed at different times and Reynolds numbers, with respect to the two obstacles assumed against the fluid flow. The other goal is to study the influence of such blocks on the Sherwood number.

2. PHYSICAL MODELING

In this study, an incompressible free fluid flow has been investigated over a plate with two square blocks, as shown in Figure 1. The dimensions of blocks over the surface are supposed to be smaller than the thickness of the boundary layer, and thus the velocity profile can be considered to be linear. The fluid enters through the inlet with the concentration of C_0. The fluid flow is assumed to be laminar. In some applications such as wind blows over the buildings, this is a valid assumption, because the air velocity is not very high and flow stands in the range of laminar regime, according to the definition of Reynolds number (see section 3.1).
A contaminant source (located in the distance of S from the inlet), dispenses the contamination with the concentration of C_W. The contaminant density is considered to be equal to that of the fluid density, and therefore, the buoyant force caused by the concentration gradient is neglected. The flow is assumed to be laminar. L, the distance between the inlet and the outlet and H, the distance between the upper boundary and the horizontal plate, must be chosen to be large enough to avoid local variations caused by the presence of the blocks and also the contaminant source. In order to do this, we choose the upper bound to be at $H=8$ and the outlet boundary to be $L=31$ (H and L are made dimensionless with respect to the first block height, h).
The first block is placed at the distance of $X=9$ *to* $X=10$, ($X=x/h$) and the second block is located at the distance of $X=11$ to $X=12$, where X is the dimensionless distance

from the inlet. The position of blocks and h are constant through this work.

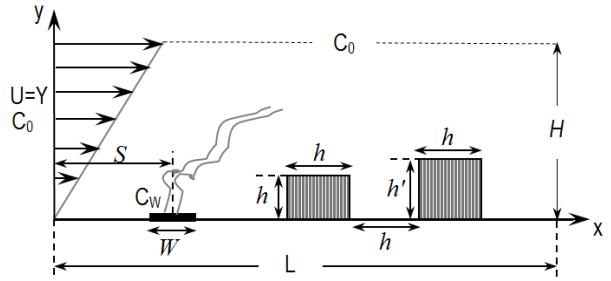

Figure 1. Schematic of contaminant dispersion over two blocks

3. MATHEMATICAL MODELING

3.1. Governing Equations The governing equations in the Cartesian coordinate system for two-dimensional incompressible flow of Newtonian fluid with constant properties in non-dimensional form are written as follows:

Continuity:

$$\frac{\partial U}{\partial X}+\frac{\partial V}{\partial Y}=0 \tag{1}$$

X-Momentum:

$$U\frac{\partial U}{\partial X}+V\frac{\partial U}{\partial Y}=-\frac{\partial P}{\partial X}+\frac{1}{\mathrm{Re}}\left(\frac{\partial^2 U}{\partial X^2}+\frac{\partial^2 U}{\partial Y^2}\right) \tag{2}$$

Y-Momentum:

$$U\frac{\partial V}{\partial X}+V\frac{\partial V}{\partial Y}=-\frac{\partial P}{\partial Y}+\frac{1}{\mathrm{Re}}\left(\frac{\partial^2 V}{\partial X^2}+\frac{\partial^2 V}{\partial Y^2}\right) \tag{3}$$

Concentration:

$$\frac{\partial C}{\partial \tau}+U\frac{\partial C}{\partial X}+V\frac{\partial C}{\partial Y}=\frac{1}{\mathrm{Re}.Sc}\left(\frac{\partial^2 C}{\partial X^2}+\frac{\partial^2 C}{\partial Y^2}\right) \tag{4}$$

The equations have been made dimensionless according to the first block height (h) and the free stream velocity (u_0). The following relations are used to make the equations dimensionless:

$$X=\frac{x}{h},\quad Y=\frac{y}{h},\quad \tau=\frac{u_o t}{h},\quad U=\frac{u}{u_o},\quad V=\frac{v}{u_o}$$
$$P=\frac{p}{\rho u_o^{\,2}},\qquad C=\frac{c-c_0}{c_w-c_0} \tag{5}$$

where u, v, p, ρ, c and t are x-velocity, y-velocity, pressure, density, concentration, and time, respectively. The indices 0 and w, correspondingly, are used for free stream and near contamination source concentration.

$Sc = \upsilon / D$ and $Re=u_0\, h / \upsilon$ are Schmidt and Reynolds numbers, respectively. Here υ is the kinematic viscosity of fluid.

The mass transfer rate is stated using the Sherwood number. Considering the non-dimensional values, the local Sherwood number (Sh) becomes:

$$Sh=-\frac{\partial C}{\partial Y}\Big|_{Y=0} \tag{6}$$

Since all the walls are isolated, except for the source, by integrating the above equation over the concentration source surface, the average Sherwood number can be calculated as follow:

$$\overline{Sh}=\frac{1}{W}\int\left(-\frac{\partial C}{\partial Y}\right)_{Y=0} dX \tag{7}$$

where W is the dimensionless length of the contaminant source.

3. 2. Initial and Boundry Conditions The boundary conditions are as follows: no-slip on the walls ($U,V=0$), linear velocity at the inlet ($U=Y$ and $V=0$) and constant pressure at the outlet and at the upper boundary placed at dimensionless height of H ($\partial V/\partial Y=0$). The concentration is zero at the inlet and at the upper boundary. The concentration is considered $\partial C/\partial X=0$ at the outlet and $C=1$ near the contaminant source. It should be stated that the walls and the blocks do not allow any mass transfer through them ($\partial C/\partial n=0$, where n is a vector perpendicular to the wall or blocks surface at any point) At the instant $t=0$, i.e. when no contaminant is dispersed by the source, the concentration is constant through the domain and equal to c_0 (the passing fluid concentration) and the dimensionless concentration is zero. In the case of velocity field, the momentum equation is steady (has no time-dependent term) and hence can be started from inflow boundary condition (i.e. linear velocity profile) to reach the steady state pattern. In addition, since the concentration equation is decoupled from the momentum equations, this equation can be solve independent of the flow filed. Hence the hydraulic conditions for solving the unsteady concentration equation would be the velocity distribution obtained from the solution of steady continuity and momentum equations.

4. NUMERICAL METHOD

The above governing equations of the incompressible viscous laminar flow along with the boundary conditions are solved by the finite volume- technique for the convective terms.

To alter the governing equations into a practical scheme of computation, they are expressed in the discretized form on a structured grid arrangement. Since the problem is solved using Cartesian coordinate system, a uniform mesh with the gridlines parallel to X and Y coordinates has been chosen. The grid network is generated using simple algebraic relations in rectangular domain of computation bounded with the boundary conditions, without considering the obstacles. Then the grid points located on the obstacles' positions suffer very large viscosity values (respect to common air viscosity). This helps us to simply create the

computational domain while the blocks are defined as solid and fixed obstacles against the flow.

Introducing a general variable φ the steady stare conservative form of all fluid flow equations, including equation for pollutant concentration can be written in the following form:

$$\frac{\partial}{\partial x_j}\left(\rho u_j \varphi\right) = \frac{\partial}{\partial x_j}\left(\Gamma \frac{\partial \varphi}{\partial x_j}\right) + S \tag{8}$$

where Γ and S, respectively, are the diffusion coefficient and source term (derived from eqs. 1-4), and φ corresponds to 1, U (V) and C for continuity, momentum and concentration equations, respectively. Now, general diffusion and convection fluxes are defined as:

$$J_j = \rho u_j \varphi - \Gamma \frac{\partial \varphi}{\partial x_j} \tag{9}$$

Hence we can re-write eq. (8) as:

$$\frac{\partial J_x}{\partial x} + \frac{\partial J_y}{\partial y} = S \tag{10}$$

A staggered grid arrangement is used for the velocity components in which, scalar variables such as pressure and concentration, is evaluated at ordinary nodal points, but velocity components are calculated on staggered grids centered around the cell faces.

Integrating from eq. (10) on a control volume surrounds a sample nodal point 'p', yields:

$$\left(J_e - J_w\right)\Delta y + \left(J_n - J_s\right)\Delta x = \left(S_u + S_p \varphi_p\right)\Delta x \Delta y \tag{11}$$

where Δx and Δy are the grid size in x and y directions, respectively. Also S_p and S_u are the source term components and the subscripts w, e, n and s are used for 'p' neighbor points in two dimensions. The continuity equation is also integrated in the same manner and gives:

$$\left(\rho u\right)_e \Delta y + \left(\rho u\right)_w \Delta y + \left(\rho v\right)_n \Delta x + \left(\rho v\right)_s \Delta x = 0 \tag{12}$$

Combining two above equations, we obtain:

$$\left[J_e - \varphi_p \left(\rho u\right)_e \Delta y\right] - \left[J_w - \varphi_p \left(\rho u\right)_w \Delta y\right] + \left[J_n - \varphi_p \left(\rho v\right)_n \Delta x\right] - \left[J_s - \varphi_p \left(\rho v\right)_s \Delta x\right] = \left(S_u + S_p \varphi_p\right)\Delta x \Delta y \tag{13}$$

The convection-diffusion terms are treated by a power-law scheme. The selected scheme is the second-order of accuracy in space and first-order in time. It is sufficiently stable in each time step and converges rapidly to desired state.

Identifying the coefficients of φ in two dimensions, the equation can be written in usual general form, as:

$$a_P \varphi_P = a_E \varphi_E + a_W \varphi_W + a_N \varphi_N + a_S \varphi_S + S_u \tag{14}$$

with $a_P = a_E + a_W + a_N + a_S - S_P$. Also:

$$a_{W,S} = D_{w,s}\, max\left[0, \left(1 - 0.1\left|Pe_{w,s}\right|\right)^5\right] + max\left[F_{w,s}, 0\right]$$
$$a_{N,E} = D_{n,e}\, max\left[0, \left(1 - 0.1\left|Pe_{n,e}\right|\right)^5\right] + max\left[-F_{n,e}, 0\right] \tag{15}$$

Where:

$$D_{e,w} = \Gamma_{e,w} \Delta y / \left(\Delta x\right)_{e,w},\ D_{n,s} = \Gamma_{n,s} \Delta x / \left(\Delta y\right)_{n,s}$$
$$F_{e,w} = \left(\rho u\right)_{e,w} \Delta y,\ F_{n,s} = \left(\rho v\right)_{n,s} \Delta x \tag{16}$$

and $Pe_i = F_i / D_i$ is called Peclet number. The pressure-velocity coupling is handled by SIMPLE algorithm, which has been well-described by Patankar [12, 13]. In this method, a guessed pressure field is used to solve the momentum equations and a pressure correction equation, deduced from the continuity equation, is solved to obtain a pressure correction field which is in turn used to update the velocity and pressure fields. The algorithm has been proved to be precise and accurate for a wide range of mathematical and engineering problem.

In case of concentration equation, an additional time-dependent term is also required. The iterative procedure for steady state calculations employing SIMPLE are then applied at each time level until convergence is achieved. The convergence accuracy is up to the seventh decimal place (10^{-7}). The numerical method is implemented on a FORTRAN program.

The effect of the grid resolution is examined in order to select the appropriate grid density. Table 1. presents the results of a grid independency study which demonstrates the effects of the number of the grid points on the average Sherwood number, $\overline{Sh}$, for six different mesh combinations. According to the table, the grid size of 68x700 is found to meet the requirements for both the grid independency study and the computational time limits. The present numerical code is also validated regarding the results of another study developed by Boum *et al.* [1] at the steady state condition. Figure 2. compares the results of the present simulation with those of the Boum's study in terms of the variations of x-velocity component throughout the y direction at various x positions. The figure demonstrates a good agreement of the results.

TABLE 1 Grid independency results

Grid size	17x93	24x140	60x560	68x700	82x933	106x1400
$\overline{Sh}$	3.384	3.622	4.729	4.855	4.910	4.92

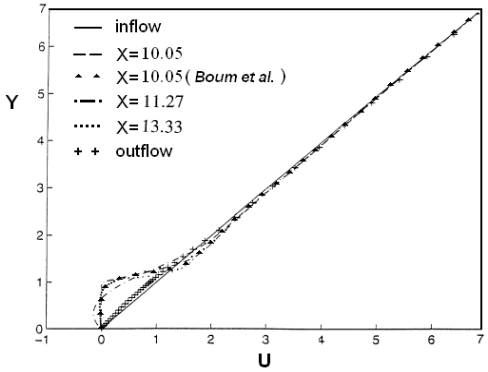

Figure 2. Validation of the results for U velocity component in y-direction, for different x-positions.

In Figure 3. the flow concentration versus *Y* in the axial position of *X=10.05* is compared with the CFD results of Boum *et al.* [1]. The purpose is to confirm the accuracy of the present numerical scheme. As it can be seen, there is again a good agreement between our results and the previously presented numerical results in the steady state condition.

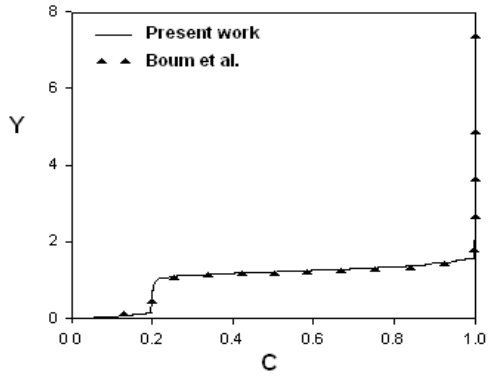

Figure 3. Concentration across the flow in steady state condition, at *X=10.05.*

5. RESULTS AND DISCUSSION

In present study, the Sherwood number is taken to be constant (*Sc=10*). The results are extended for *W=1*. The dimensionless distance between the inlet and the center of contaminant source, *S*, is set to *5.5*. The flow and the concentration lines are drawn in Figure 4.

Figure 5. illustrates the concentration of the contaminant distributed around the source and blocks in different times, after the source starts to disperse the contamination in flows with Reynolds numbers of *6* and *30*, respectively. In the calculation, the variations in Reynolds number have been assumed to be caused by changes in the ratio of u_0/h. In order to calculate the flow real time in seconds, using the dimensionless time, τ, the ratio of u_0/h has been taken as $1/s$ for *Re=6*. It is obvious that for other Reynolds numbers, the ratio of u_0/h changes in a linear way. As it can be observed in this figure, in initial instances of *t=30s* and *t=50s*, more contaminants are dispersed in higher Reynolds number. However, when the time passes and the flow becomes closer to the steady state condition, the contaminant concentration is higher for *Re=6*.

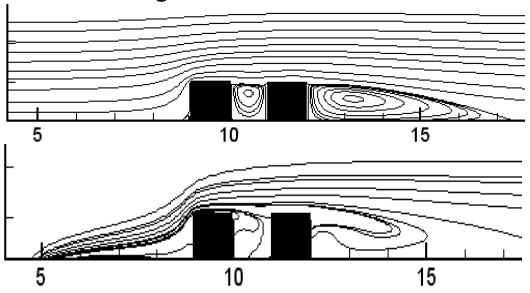

Figure 4. Streamlines and concentration lines, *W=1*, *S=5.5* and *Re=18*

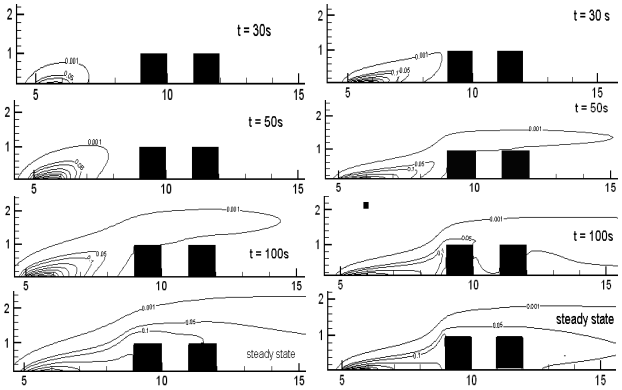

(a) *Re= 6* (b) *Re= 30*

Figure 5. The contaminant concentration distribution for various time levels at two different Reynolds numbers

In order to investigate better the subject, it would be useful to look at the average concentration remained between the blocks in this figure. It can be seen that the average concentration decreases, as the Reynolds number increases.

The average concentration accumulating between the blocks is plotted versus the time for different Reynolds numbers in Figure 6. The point mentioned for Figure 5. can be seen more obviously in this figure. In the initial instances after dispersion of the contaminating mass, the average concentration and the curve slope is greater for higher Reynolds numbers, however, a while after the starting time, the average concentration decreases with increasing the Reynolds number. The other result which can be realized from Figure 6. is that by increasing the Reynolds number, the duration required to reach to the steady state decreases, and the curve slope decreases quicker.

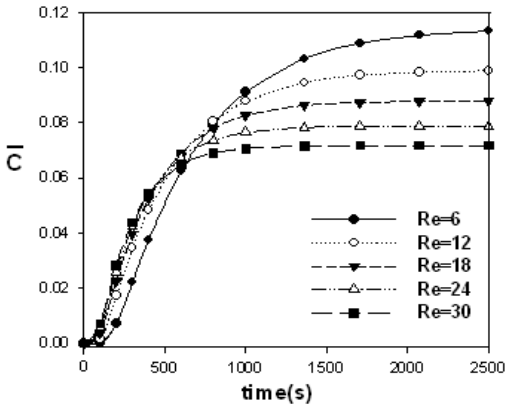

Figure 6. Average concentration over the time for different Reynolds numbers, *W=1*, *S=5.5*

In Figure 7. the average Sherwood number has been plotted versus S for different Reynolds numbers. As it can be observed, by increasing the Reynolds number, the mean Sherwood number decreases. Also it can be seen that the closer the concentration source is to the block, the lower the Sherwood number is. Decreasing the Sherwood number is gradual for low S, but in *S=7.5*

and more specifically in *S=8.5* (in which the source is adjacent to the block), the Sherwood number decreases suddenly. This can be contributed to the block's effects on the flow lines and therefore on the amount of mass transferred from the source.

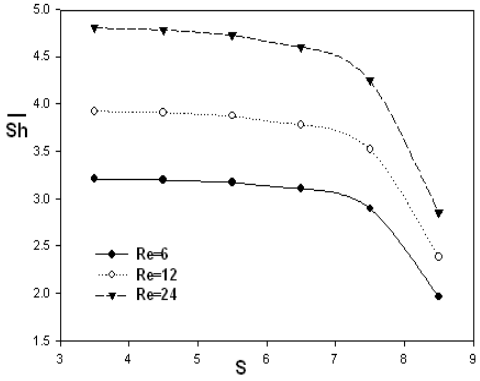

Figure 7. Average Sherwood number versus S for different Reynolds numbers

Figure 8. shows the effect of distance between the inlet and the center of contaminant source on the average concentration accumulated between the blocks, in different Reynolds numbers. It can be seen from this graph that the closer the contaminant source is to the blocks, the higher the mean concentration accumulating between two blocks is. When the source is in the middle point of the blocks, the mean concentration decreases because the Sherwood number decreases.

The effect of changing the contaminant source length can be also investigated through the previously mentioned parameters. In order to do this, by keeping the final point of source on *X=7*, its initial point changes. For example, the initial point is calculated to be *X=6.5* for *W=0.5*. It may be notable that the distance between the final point of the contaminant source and the blocks is always constant. As it could be predicted, by increasing W, the mean Sherwood number decreases (Figure 9). while the mean concentration increases (Figure 10). It can be seen that the duration the contaminants reach to the blocks does not changed greatly, because the distance between the final point of the source and the first block is constant.

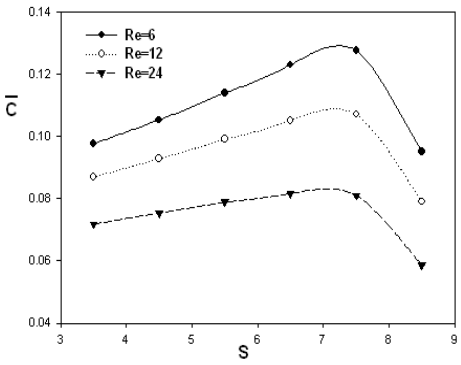

Figure 8. Average concentration accumulated between the blocks versus *S* in different Reynolds numbers

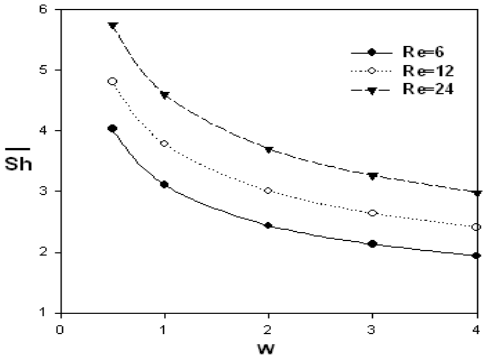

Figure 9. Average Sherwood number versus *W* for different *Re* numbers

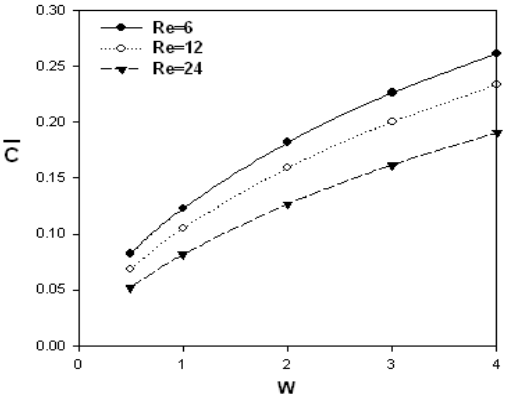

Figure 10. Average concentration accumulated between the blocks versus *W* for different *Re* numbers

Figure 11. depicts the variation of average Sherwood number in case of time for different source lengths. The figure is plotted for *Re=12*. The source endpoint is located at *X=7* for all graph lines. As illustrated in this figure, the time the Sherwood number reaches to its steady state value reduces with the decrement of the source length. Moreover, regarding the figure, it is clear that generally, the steady state condition over the source happens earlier than other geometrical places.

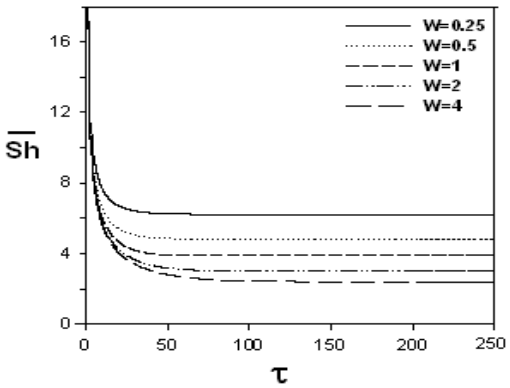

Figure 11. Average Sherwood number versus time for different source lengths, *Re=12*

The effect of a block on the streamlines for different Reynolds numbers can be seen in Figure 12. In this figure, the re-circulating zone after the block growths with the Reynolds number is clearly shown. This issue

is also confirmed by the recirculation length which is plotted in Figure 13. The distance between the block and the surface crossing the streamline is selected as the recirculation length, L_R. For example, this value is equal to *4* for *Re=12*. The relationship between the Reynolds number and the recirculation length, L_R, is linear, as shown in Figure 13.

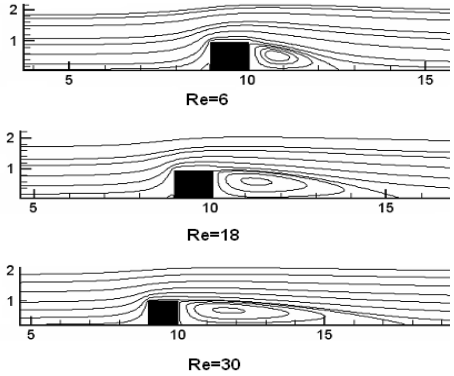

Figure 12. Effect of a block on the streamlines in different Reynolds numbers

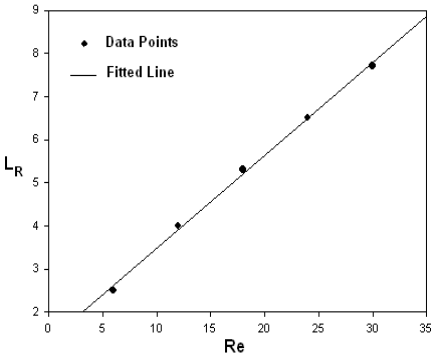

Figure 13 Recirculation-zone length behind the block versus Reynolds number

Figure 14. demonstrates the local Sherwood number over the source for different Reynolds numbers. The local Sherwood number over the source represents the amount of mass transfer from it. In the case of free convection flows, it is expected that the minimum Sherwood number happens at the middle points of the source, however in this case, it is minimized somewhere near the right end of the source, as it can be seen in Figure 14. due to the flow direction and velocity.

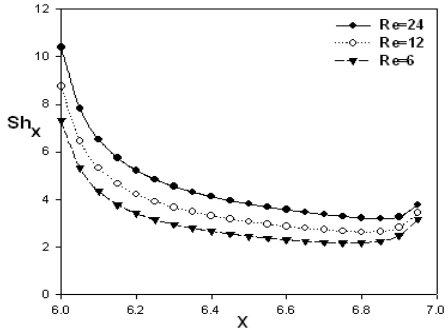

Figure 14. Local Sherwood number over the contaminant source at different Reynolds numbers, *W=1*, *S=6.5*

Different height blocks: The streamlines for the flow over the blocks with different heights is showed in Figure 15a. The Reynolds number is set to *Re=12* and the graph is presented for a wide range of block height ratio from R_h*=0.5* to *1.5*, where $R_h=h / h'$. By increasing the height of the first block in the flow direction, the recirculation occurring between the blocks is growing. Furthermore, when the block heights ratio passed the unity, the height of the first block that enlarges the recirculation length occurs after the second block.

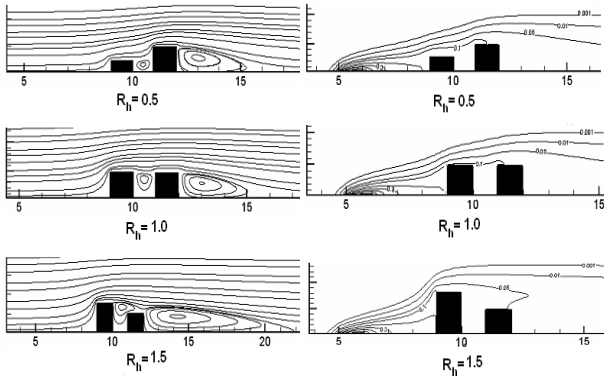

(a) Streamlines (b) Concentration

Figure 15. Steady state flow streamline and concentration over two blocks with different heights, *Re=12*, *S=5.5*, *W=1*

Figure 15b. also depicts the concentration lines for the same conditions. The source location is from *X=5* to *X=6*. By increasing the height of the first block (in the flow direction) especially after R_h*=1*, the contaminant concentration increases near the left wall of the first block, and moves slowly upward. This phenomenon can be interpreted by the shape of the streamlines in this position which can be observed in Figure 15a. where the velocity vertical component grows by ascending the first block height, while the *x*-velocity component decreases.

Figure 16. illustrates the effect of block height ratio (R_h) on the time of reaching the contaminant to the blocks. Each time index from 1 to 4 belongs to a block wall from left to right, respectively, as they can be observed in Figure 15. This graph is plotted for *Re=12*, *W=1* and *S=5.5*. Regarding the time for the contaminant to reach the left block walls, τ_1 and τ_2, the time in which the concentration of one of the primary cells from *Y=0* to *Y=1* reaches the value of *C=0.0001*, is selected as the criterion. It can be clearly seen that for all times, an ascending trend is observed, though the slopes of the lines are different for each time. The effect of the block's height on the time for the arrival of the contaminant can be explained by the streamlines configuration around the blocks, regarding the fact that following the fluid velocity vectors, the contaminant dispersion from the source will not affect the shape of the streamlines. For all of the height ratios, the average dimensionless time is greater than τ_1 and τ_2, as shown in Figure 16. The reason for this is that the contaminant

passing from *Y=0.25* to *Y=1* can reach to the region between the blocks from the top of the blocks. For the right block walls, it is seen that the times τ_3 and τ_4 are at first greater than the average, but they fall below the average by increasing the blocks height ratio. The reason can be described again by the means of the configuration of the streamlines. For small height ratios, the first block does not prevent the contaminant from reaching to the second block and most of the streamlines keep straight. Therefore, the average time remains below the arrival times of the contaminant to the second block. However by increasing the height of the first block and consequently the height ratio, R_h, especially after $R_h=1$, the left block obstructs the way of getting the contaminant to the right block, and, as a result, the times τ_3 and τ_4 will be less than the average time. It is also observed that the time τ_2 belongs to the right wall of the first block increases far and away in high height ratios. This trend indicates that the contaminant reaches to this wall rarely and after a long time. This is due to the shape of recirculation zone happens between the blocks. Therefore, this position may be introduced as a safe zone.

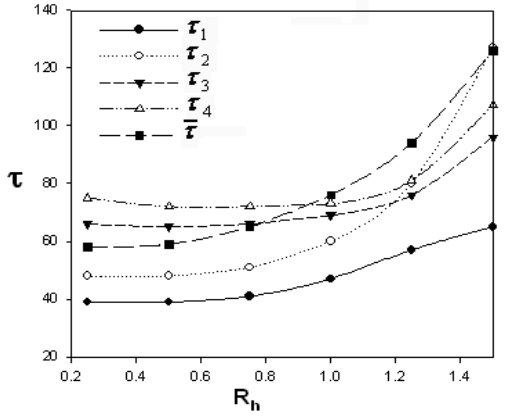

Figure 16. The time to reach the contaminant to the blocks versus the blocks height ratio, *Re=12*, *S=5.5*, *W=1*

6. CONCLUSIONS

In this study, the problem of incompressible air flow over two blocks in the presence of a contaminant source was simulated numerically in both steady and unsteady conditions. The results indicates that by increasing the inflow Reynolds number, the time the contamination reaches the blocks, the mass transfer from the contaminant source, and the Sherwood number increase, while the amount of the contaminant accumulating between the two blocks decreases in the steady state. It has also been shown that in higher Reynolds numbers, the contaminant concentration distribution reaches to its steady state more quickly. Also, it can be observed that while the contaminant source gets closer to the blocks, the Sherwood number and the concentration decrease gradually, however, when the source becomes adjacent to the first block, the Sherwood number and concentration suddenly decrease.

The flow over two blocks with different heights has been also investigated in the unsteady condition. With increasing the height of the first block in the flow direction, the re-circulation occurring between the blocks grows. For small height ratios, the first block does not prevent the contaminant from reaching the second block. Therefore, the average time remains below the arrival time of the contaminant to the second block. However, by increasing the height ratio, a reverse trend is expected.

It is also observed that the time τ_2 which belongs to the right wall of the first block increases far and away in high height ratios. This trend indicates that the contaminant reaches this wall rarely, after a long time. This is due to the shape of re-circulation zone existing between the blocks. Therefore, this position may be introduced as a safe zone.

REFERENCES

1. Boum, G.B.N., Martemianov, S. and Alemany, A., "Computational study of laminar flow and mass transfer a surface-mounted obstacle", ***International Journal of Heat and Mass Transfer,*** Vol. 42, No. 15, (1999), 2849-2861.
2. Hancu, S.A.L., Ghinda, T.A., Ma, L.C., Lesnic, D.B. and Ingham, D.B.B., "Numerical modelling and experimental investigation of the fluid flow and contaminant dispersion in a channel", ***International Journal of Heat and Mass Transfer,*** Vol. 45, No. 13, (2002), 2707–2718.
3. Hayashia, T., Ishizub, Y., Katoa, S., Murakamia, S., "CFD analysis on characteristics of contaminated indoor air ventilation and its application in the evaluation of the effects of contaminant inhalation by a human occupant", ***Journal of Building and Environment,*** Vol. 37, No. 3, (2002), 219–230.
4. Gadgil, A.J., Lobscheid, C., Abadie, M.O. and Finlayson, E.U., "Indoor pollutant mixing time in an isothermal closed room: an investigation using CFD", ***Journal of Atmospheric Environment,*** Vol. 37, (2003), 5577–5586.
5. Kaya, A., Aydin, O. and Dincer, I., "Experimental and numerical investigation of heat and mass transfer during drying of Hayward kiwi fruits, Actinidia Deliciosa Planch", ***Journal of Food Engineering,*** Vol. 88, No. 3, (2008), 323–330.
6. Deng, Q.H., Zhou, J., Mei, C. and Shen, Y.M., "Fluid, heat and contaminant transport structures of laminar double-diffusive mixed convection in a two-dimensional ventilated enclosure", ***International Journal of Heat and Mass Transfer,*** Vol. 47, No. 24, (2004), 5257–5269.
7. Clear, R.D., Gartland, L. and Winkelmann, F., "An empirical correlation for the outside convective air-film coefficient for horizontal roofs", ***Journal of Energy and Buildings,*** Vol. 35, No. 8, (2003), 797–811.
8. Kaya, A., Aydin, O. and Dincer, I., "Numerical modeling of heat and mass transfer during forced convection drying of cylindrical moist objects", ***Journal of Numerical Heat Transfer,*** Vol. 51, No. 9, (2007), 843–854.
9. Kaya, A., Aydin, O. and Dincer, I., "Heat and mass transfer modeling of recirculating flows during air drying of moist objects for various dryer configurations", ***Journal of Numerical Heat Transfer,*** Vol. 53, No. 1, (2008), 18-34.

10. Xamán, J., Ortiz, A., Álvarez, G. and Chávez, Y., "Effect of a contaminant source (CO2) on the air quality in a ventilated room", ***Journal of Energy,*** Vol. 36, (2011), 3302–3318.
11. Pal, D. and Mondal, H., "Effects of Soret Dufour, chemical reaction and thermal radiation on MHD non-Darcy unsteady mixed convective heat and mass transfer over a stretching sheet", ***Communications in Nonlinear Science and Numerical Simulation,*** Vol. 16, No. 4, (2011), 1942–1958.
12. Patankar, S.V., "Numerical heat transfer and fluid flow". Washington DC, Hemisphere Publication Corporation, (1980).
13. Patankar, S.V., "Computation of Conduction and duct flow heat transfer innovative", USA: Resaerch Inc., (1991).